



## Efficient Feature Extraction and Selection Model for Tumor Detection and Classification in Medical Imaging

Cherifa Nabila Chaoui<sup>1\*</sup>Boudjelal Meftah<sup>1</sup>Abdelghani Ghomari<sup>2</sup>

<sup>1</sup>LISYS Laboratory, Department of Computer Science, Faculty of Exact Sciences,  
University Mustapha Stambouli of Mascara, Algeria

<sup>2</sup>RIIR Laboratory, Computer Science Department, Faculty of Exact and Applied Sciences,  
University Oran1 Ahmed Ben Bella, Oran, Algeria

\*Corresponding author's Email: [nabila.inf@gmail.com](mailto:nabila.inf@gmail.com)

---

**Abstract:** Among the most advanced AI models is Computer-Aided Diagnosis (CAD). Research in this field is crucial as it enhances the efficiency and accuracy of disease detection, enabling early treatment and reducing mortality rates. To this end, we propose the development of a comprehensive CAD system capable of processing various types of medical images. The primary objective of this study is to improve the efficiency and accuracy of medical image analysis for tumor categorization and tumor type identification. This will be accomplished by employing an efficient and accurate feature extraction and selection model, ensuring error-free classification results while minimizing computation time. Our proposed model is structured into two main components: optimal feature extraction and selection, and classification. In the first part, the Histogram of Oriented Gradients (HOG) method is employed for feature extraction, while the Binary Cuckoo Search (BCS) algorithm is utilized to optimize these features. In the second part, the optimized features are input into the Optimal-Path Forest (OPF) classifier to effectively perform the classification task. Based on the experimental results, We conclude that this hybrid approach achieves exceptional performance with minimal computational time (9.604 seconds for breast images and 13.740 seconds for brain images). Specifically, the proposed HOG-BCS-OPF model achieves high accuracy rates of 99.73%, 97.31%, and 93.85% for the breast X-ray datasets: DDSM, INbreast, and MIAS, respectively, and 97.72%, 93.57% for the Figshare and Kaggle brain MRI dataset, outperforming the state-of-the-art techniques cited in Section 5 of this paper. These results underline the robustness, reliability, and effectiveness of our proposed model, highlighting its potential as a powerful and timely tool for tumor detection and classification in medical imaging.

**Keywords:** Feature extraction, Tumor detection, Binary Cuckoo search, Optimum path forest, Medical images.

---

### 1. Introduction

Cancer is the leading cause of death globally, with over 200 types, making it a critical public health challenge [1-3]. While improving treatment remains a priority, early and accurate diagnosis through medical imaging is now a key focus. However, diagnosis is time-consuming and relies heavily on radiologists' expertise, creating opportunities for computer scientists to advance tumor diagnosis through innovative imaging technologies [4-8]. Medical images require precise analysis and processing to extract meaningful information for

accurate diagnosis. Errors in diagnostic systems are unacceptable, as they can lead to flawed decisions and fatal outcomes. Despite progress, CAD systems still face challenges and limitations [9, 10].

Superior feature extraction and selection methods are crucial for achieving accurate and reliable image classification, enabling the development of robust CAD systems. These systems provide detailed insights into patient conditions, enhancing diagnostic accuracy and improving outcomes.

#### Problem specification

Currently, CAD systems are widely used for detecting and diagnosing brain, breast, and lung diseases [9], with this study focusing on brain and

mammographic images due to their clinical significance. CAD development involves processing medical images to extract essential features [11, 8], which are then used to identify anomalies [7, 12]. However, the complexity and variability of medical data require optimal feature extraction and thorough analysis to create efficient, cost-effective, robust, and reliable diagnostic methodologies.

To perform tumor detection and classification in breast images, researchers cited in references [8, 13-16] have developed deep learning-based methods, while others [49-52] proposed the graph convolutional network (GCN) technique that exploit the characteristics of a node in the breast image and its location to carry out predictions. The results show high accuracy and an 85% reduction in error rates, while also enabling the processing of graph-structured data—a capability lacking in traditional methods such as Support Vector Machines (SVM), K-Nearest Neighbors (KNN), Decision Trees (DT), and Bayesian algorithms. These conventional techniques remain unsuitable for large datasets and continue to struggle with class overlap. However, these methods are computationally demanding, struggle with generalization to new datasets, and are sensitive to variations in image acquisition and patient demographics. Additionally, they are still limited due to the need for large amounts of well-annotated data, posing challenges for their practical implementation.

Recently, several techniques have been used for brain tumor detection and classification using magnetic resonance image (MRI), such as Convolutional Neural Networks (CNNs), Vision Transformers (ViTs) dedicated to feature extraction by exploiting a self-attention mechanism to gather global contextual information from the whole image and the Swin Transformers that uses hierarchical feature maps to efficiently represent different levels of features in images [1, 2, 15, 19, 61-63], offering superior accuracy and automatic feature extraction compared to classical machine learning methods that require manual feature extraction such as artificial neural network (ANN), watershed algorithm (WA), region growing algorithm (RGA), which provide global characteristics of the images as they still risk giving over-segmentation of the images. However, CNNs, ViTs and Swin Transformers are highly data-dependent, needing large volumes of labeled training data, which is challenging to obtain in medical imaging. Insufficient data can reduce accuracy, and they also demand significant computational resources, including high RAM and GPUs, making them more resource-intensive than machine learning methods.

The analysis of prior research has led to the formulation of the following key research questions:

How can challenges in tumor detection and classification in medical imaging be effectively addressed?

How can an efficient, robust, and accurate classification approach be developed for widespread use in CAD systems?

Is it possible to create a universal and comprehensive classification method applicable to all types of medical images?

What formal feature extraction approach can produce meaningful, reliable, and insightful hand-crafted attributes while minimizing information loss and avoiding the limitations of CNNs?

Which bio-inspired approaches are best suited for optimizing feature extraction and tumor classification, achieving high accuracy with reduced training time and fewer samples?

#### Motivation and Contribution

This paper proposes efficient bio-inspired methodologies to address the limitations of CNNs in medical imaging. These approaches aim to extract optimal features, enabling highly accurate tumor classification with fewer training samples and reduced training time. The research focuses on enhancing the efficiency and accuracy of medical imaging for tumor categorization and type identification using advanced AI algorithms. By leveraging bio-inspired techniques, the study aims to provide a robust and scalable solution to improve diagnostic outcomes.

Our contribution centers on tumor detection and classification in medical images using an efficient and accurate feature extraction approach. We propose a mathematical formalization based on the Histogram of Oriented Gradients (HOG) descriptor [20], which excels due to its operation on localized cells, ensuring invariance to geometric and photometric transformations. This makes HOG particularly effective for capturing robust and meaningful features in medical imaging.

To enhance the robustness of our approach, we propose integrating a feature optimization step after feature extraction to address overfitting, reduce computational time, and improve classification accuracy. We employ the Cuckoo Search (CS) algorithm [21], a nature-inspired metaheuristic based on cuckoo brood parasitism [22, 23]. A binary variant, Binary Cuckoo Search (BCS) [21], is used for feature optimization, marking the first application of the HOG-BCS combination in medical imaging, which serves to best avoid the drawbacks of each conventional technique, particularly in terms of images over-segmentation, optimal performance and

in minimizing computational time and hardware compared to CNNs and their competitive alternative: ViTs, Swin Transformers and GCNs techniques. BCS outperforms other algorithms like Firefly Algorithm (FA), Bat Algorithm (BA), and Particle Swarm Optimization (PSO) in feature selection, addressing the limited focus on bio-inspired algorithms in this domain.

The final step of the proposed workflow involves classification using the optimized features from the feature optimization step. We employ the OPF algorithm [24], a robust and efficient machine learning technique widely used in computer vision. OPF is advantageous due to its noise tolerance, low computational time, and lack of sensitive parameters. It outperforms SVM in efficiency [25] and is versatile, handling supervised, unsupervised, and semi-supervised tasks. OPF also provides interpretable results, graphical representations of optimal paths, and supports both binary and multiclass classification, making it highly effective for medical image analysis [26].

The primary advantage of our proposed approach is its ability to generate optimal, accurate, and relevant features, resulting in highly reliable and precise image classification. The tumor detection and classification model are universally applicable, seamlessly adaptable to various medical images, such as mammographic, cervical, and pulmonary. Additionally, it reduces the diagnostic burden on healthcare professionals by streamlining disease diagnosis, treatment planning, and patient monitoring, ultimately improving clinical workflows and patient care outcomes.

Our major contributions, based on a thorough review and comparison of recent approaches for tumor detection and classification in medical images, are summarized as follows:

### 1) Histogram of Oriented Gradients (HOG) for Feature Extraction:

- We propose using HOG, a formal mathematical approach, to robustly and accurately extract shape, texture, and contour information from medical images.
- HOG automatically generates meaningful, detailed, and reliable features without manual engineering, making it ideal for medical imaging due to its:
  - Noise tolerance.
  - Immunity to photometric and geometric transformations.
- Ability to capture shape/contour information.
- Computational efficiency and simplicity.

- Unsupervised feature extraction (no labeled data required).

### 2) Binary Cuckoo Search (BCS) for Feature Selection:

- We introduce BCS, a bio-inspired algorithm, to optimize feature selection, ensuring highly accurate and reliable features.
- BCS reduces computational costs and processing time, enhancing workflow efficiency.

### 3) Optimal-Path Forest (OPF) for Classification:

We recommend OPF for classifying the optimized features, leveraging its advantages:

- Efficient handling of large datasets.
- No prior knowledge of clusters required (unsupervised capability).
- Faster training compared to traditional methods.
- Minimal hyperparameter tuning.
- No assumption of feature space separability.
- OPF ensures robust, accurate, and efficient classification in medical imaging.

These contributions collectively enhance the accuracy, reliability, and efficiency of tumor detection and classification in medical imaging.

This paper is structured as follows: Section 2 provides a concise overview of the proposed model architecture for tumor detection and classification in medical images. Section 3 elaborates on the proposed model for feature extraction and selection in medical images. Section 4 describes the proposed model for medical image classification using the OPF algorithm. Section 5 presents and evaluates the experimental results obtained. Finally, Section 6 outlines the conclusions drawn from this study and discusses potential directions for future work.

## 2. Overall architecture's overview of the proposed model for tumors detection and classification in medical image

A review of existing methods for tumor detection and classification in medical images shows that many rely on general-purpose deep learning classifiers. While effective, these methods require large amounts of training data and substantial computational resources, leading to high complexity and limited scalability for multi-sample or institutional datasets. To overcome these challenges, this section presents the design of the proposed model for tumor detection and classification, as illustrated in Fig. 1.

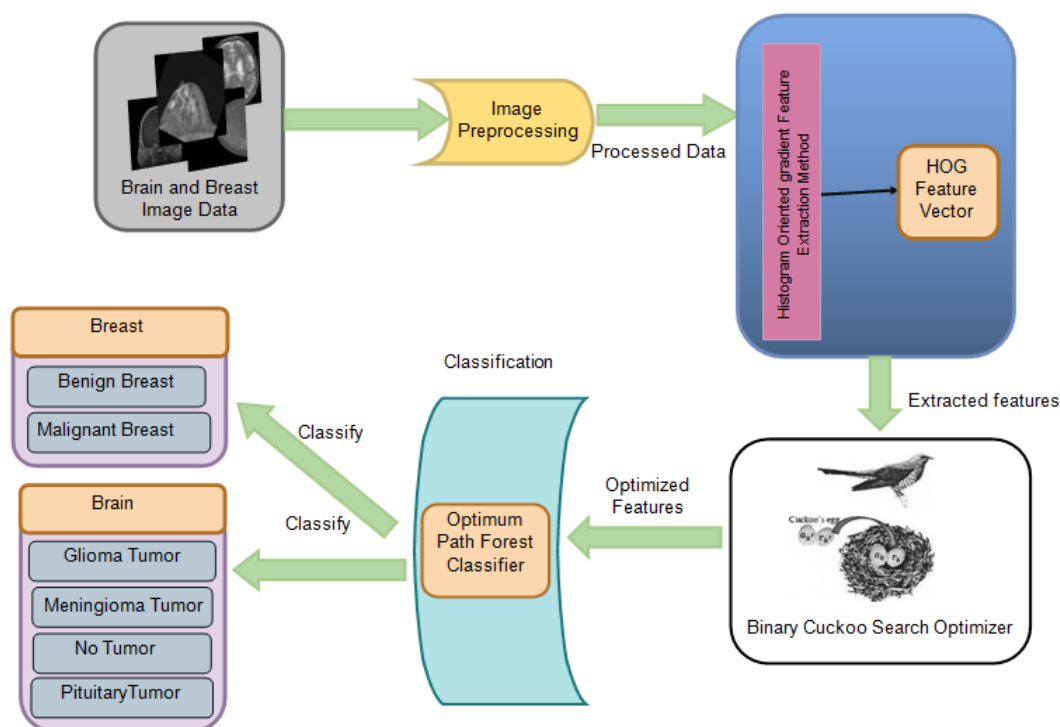


Figure. 1 Proposed model architecture for tumor detection and classification in medical images

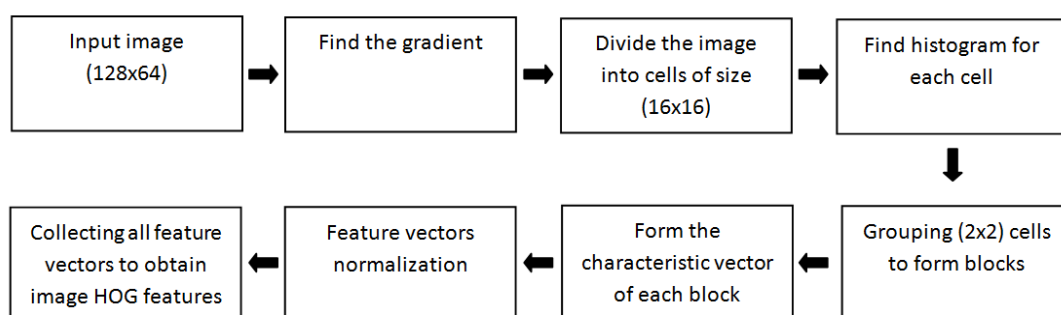


Figure. 2 HOG feature extraction operating steps

The proposed model addresses the limitations of traditional methods by combining efficient feature extraction, optimization, and classification techniques. Using Histogram of Oriented Gradients (HOG) for feature extraction, Binary Cuckoo Search (BCS) for feature optimization, and Optimal-Path Forest (OPF) for classification, the model achieves high accuracy and robustness while minimizing computational time and data requirements. This scalable and versatile approach is well-suited for diverse medical imaging datasets, offering a practical solution for real-world clinical applications.

From the architecture, the input images fall into two distinct categories, demonstrating that the classification model processes different image types based on the input provided. In this study, brain and mammographic images are used to showcase the model's effectiveness. To enhance performance and reliability, the original image undergoes

preprocessing to improve quality. The HOG descriptor is then applied to extract features effectively, followed by optimization using the BCS algorithm to increase accuracy, robustness, and speed. Finally, the OPF algorithm classifies the images into their respective categories.

### 3. Proposed model for feature extraction and selection in medical images

The preprocessed image is analyzed using the HOG descriptor, which captures precise pixel-level details to extract accurate and meaningful features, generating a comprehensive feature vector. However, processing large feature spaces can be computationally intensive. To address this, the BCS algorithm optimizes the feature set by reducing dimensionality, ensuring optimal feature selection for improved accuracy and efficiency in medical image

classification. The following sections provide a detailed explanation of the feature extraction and feature selection steps.

- Feature Extraction through Histogram of Oriented Gradients

The HOG descriptor, introduced by Dalal and Triggs [27], characterizes objects in an image by analyzing the distribution of gradient intensities or edge directions. It works by dividing the image into small cells, computing a histogram of gradient orientations for each cell, and combining these histograms into a final descriptor. The process involves four main steps:

- 1) computing gradient magnitude and angle matrices,
- 2) dividing the image into cells,
- 3) generating nine-bin histograms for each cell, and
- 4) grouping cells into overlapping blocks, normalizing histograms, and concatenating them to form the feature vector.

The figure below illustrates the key steps involved in the HOG operation.

- Best features selection through Binary Cuckoo Search algorithm

As highlighted in the introduction, the classification step can be time-consuming and resource-intensive, especially when feature extraction is unoptimized. This is particularly problematic for datasets with many features, where redundancy, irrelevance, or noise may exist. To tackle this, a nature-inspired optimization technique is used to treat feature selection as an optimization problem, identifying the most relevant features to create an optimal subset. By reducing feature space dimensionality, this approach boosts classification accuracy and computational efficiency, making the system more practical for real-world use.

To address feature optimization, we use an algorithm inspired by the parasitic behavior of cuckoo birds, which lay their eggs in host nests, mimicking the host eggs' appearance. If detected, the host may discard the egg or abandon the nest. This behavior inspired the Cuckoo Search (CS) algorithm, developed by Yang and Deb [28], which operates on three key rules:

- 1) Random Nest Selection: Each cuckoo randomly chooses a nest to lay its eggs.
- 2) Survival of the Fittest: Only nests with high-quality eggs are retained for future generations, as the number of host nests is fixed.

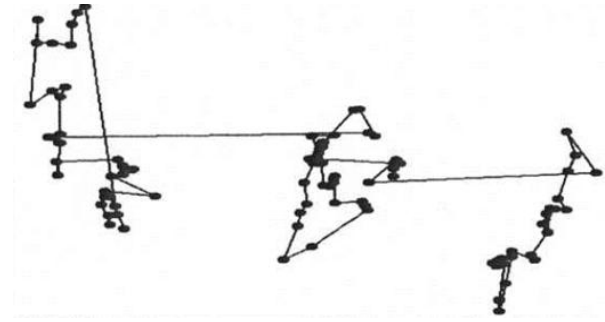


Figure. 3 Random walk via Lévy flights

- 3) Host Discovery and Nest Abandonment: If a host identifies the cuckoo's egg, it may discard the egg or abandon the nest to build a new one elsewhere.

Algorithmically, each host nest  $n$  is defined as an agent that can hold a single egg  $x$  (for one-dimensional problems) or multiple eggs (for multi-dimensional problems). The CS algorithm begins by randomly placing the nest population in the search space. At each iteration, the nests are updated. The probability of a cuckoo egg being detected by the host bird is  $p_a \in [0,1]$  [29]. The prediction of the next location depends on both the transition probability and the current location, making the path to the cuckoo nest a random walk. Step lengths are determined using a heavy-tailed probability distribution, and the probability of selected destinations is predicted using Lévy flight behavior, as illustrated in Fig. 3.

The implementation of the random walk with Lévy flights is a key component of the CS algorithm. Lévy flights are a type of random walk where the step lengths follow a heavy-tailed probability distribution, enabling both local and global exploration of the search space.

The implementation steps for the random walk using Lévy flights are as follows:

- 1) **Initialize Parameters:**

- Define the number of nests (solutions)  $n$ .
- Set the probability  $p_a$  of a host bird detecting a cuckoo egg (typically  $p_a \in [0,1]$ ).
- Define the maximum number of iterations  $T$ .

- 2) **Generate Initial Population:**

- Randomly initialize the positions of the nests (solutions) in the search space.

- 3) **Lévy Flight Step Generation:**

- For each nest  $i$ , generate a new solution  $x_i(t+1)$  using Lévy flight

$$X_i(t+1) = X_i(t) + \alpha \oplus \text{Lévy}(\lambda) \quad (1)$$

where:

- $X_i$ : Current position of the nest.
- $\alpha$ : Step size scaling factor (controls the step length).
- $\oplus$ : Entry-wise multiplication.
- $\text{Lévy}(\lambda)$ : Random step length drawn from a Lévy distribution with parameter  $\lambda$ .

#### 4) Lévy Distribution:

- The Lévy distribution is characterized by heavy tails, allowing for occasional large jumps. The step length  $s$  is computed as:

$$s = \frac{u}{|w|^{1/\beta}} \quad (2)$$

where:

- $u$  and  $w$  are drawn from normal distributions:

$$\begin{cases} u \sim N(0, \sigma_u^2) \\ w \sim N(0, \sigma_w^2) \end{cases} \quad (3)$$

where  $\sigma_u$  and  $\sigma_w$  are obtained from the following formula:

$$\begin{cases} \sigma_u = \left( \frac{\Gamma(1+\beta) \sin(\beta\pi/2)}{\Gamma((1+\beta)/2) \beta 2^{(\beta-1)/2}} \right)^{1/\beta} \\ \sigma_w = 1 \end{cases} \quad (4)$$

$\beta$  is a parameter typically set to 1.5.

#### 5) Update Nests:

- Evaluate the fitness of the new solutions  $X_i(t+1)$ .
- Compare the new solutions with the current ones and keep the better solutions based on fitness.

#### 6) Host Discovery and Nest Abandonment:

- With probability  $p_a$ , abandon the worst nests and replace them with new random solutions.

#### 7) Repeat:

- Repeat steps 3–6 until the maximum number of iterations  $T$  is reached or a stopping criterion is met.

In traditional CS, solutions are updated to continuous-valued positions in the search space. However, in BCS for feature selection, the search space is modeled as an  $n$ -dimensional Boolean lattice, where solutions are updated across the corners of a hypercube. Since feature selection involves deciding whether to include or exclude a feature, a binary solution vector is used:

- 1 indicates the feature is selected for the new dataset.

- 0 indicates the feature is excluded.

To ensure solutions remain binary, a test formula (5) is applied, restricting updates to binary values within the Boolean lattice. This adaptation makes BCS suitable for feature selection tasks.

$$X_i = \begin{cases} 1 & X_i \text{ selects the } j\text{th characteristic} \\ 0 & \text{Otherwise} \end{cases} \quad (5)$$

To extend the cuckoo algorithm to discrete binary regions, the original cuckoo method incorporates mapping functions (6) and (7) as follows:

$$\text{sig}(\text{step}) = \frac{1}{1+e^{-\gamma \text{step}}}, \gamma = 1 \quad (6)$$

$$X_i(t) = \begin{cases} 1 & \text{rand}() \leq \text{sig}(\text{step}) \\ 0 & \text{Otherwise} \end{cases} \quad (7)$$

These functions transform continuous-valued solutions into binary values, ensuring that the search space is restricted to the corners of an  $n$ -dimensional Boolean lattice. This adaptation allows the algorithm to operate effectively in binary domains, making it suitable for feature selection tasks where solutions are represented as binary vectors (e.g., 1 for selected features and 0 for excluded features).

### 4. Proposed model for medical image classification through optimum-path forest algorithm

In this section, we introduce the proposed model for medical image classification using the OPF algorithm [30], a graph-based approach that frames classification as a graph partitioning problem. The model uses the feature vectors extracted and optimized in earlier steps as input. By applying the supervised version of OPF, the model aims to achieve high accuracy and reliability in classifying medical images, particularly for tumor detection and diagnosis.

The OPF algorithm constructs a graph where nodes represent samples (defined by feature vectors) and edges are weighted by the distance between these vectors. It identifies key samples, called prototypes, which act as roots for optimal path trees. Each sample is classified based on its strongest connection to a prototype, forming an optimal path forest. This method ensures efficient, interpretable classification, making it highly suitable for medical imaging applications.

The following subsections detail the OPF algorithm and its integration into the proposed model for medical image classification.

The image is converted into a feature vector, represented as an array, using the feature descriptor from the previous section. This feature vector acts as the input for the classification process.

The learning phase of the OPF algorithm identifies the optimal set of prototypes  $P$  and constructs an OPF classifier [30] rooted at these prototypes. This involves selecting prototypes that best represent each class and using them to build optimal path trees. The resulting classifier efficiently partitions the feature space, enabling accurate and robust classification of medical images. By optimizing prototype selection, the OPF algorithm ensures an effective and computationally efficient classification process, making it a powerful tool for medical image analysis.

To achieve this, a Minimum Spanning Tree (MST) is constructed on the training data to efficiently identify the required nodes. Prototypes are selected as samples connected by edges with different labels, ensuring zero classification error during training when using the path-cost function  $f_{max}$ . This function evaluates the maximum edge weight along the path between adjacent samples labeled with different classes in the training set [31].

The learning phase aims to minimize the cost assigned to each sample, with optimality determined by the path-cost function  $f_{max}$  [32]. In the MST, each pair of samples is connected by a unique optimal path defined by  $f_{max}$ , expressed as follows:

$$f_{max}((q)) = \begin{cases} 0 & \text{if } q \in P, \\ +\infty & \text{otherwise} \end{cases} \quad (8)$$

$$f_{max}(\phi \cdot (q, u)) = \max\{f_{max}(\phi), d(q, u)\} \quad (9)$$

where  $\phi$  represents a path,  $q$  and  $u$  are samples,  $d(q, u)$  is the distance between them, and  $P$  denotes the set of prototypes.

Therefore, minimizing the cost of each training sample is guided by the optimal set of prototypes. The outcome of the training step is an optimal cost  $C(u)$  (represented by formula (10)) assigned to each sample  $u$  belongs to  $V$ , where  $V$  denotes the training set.

$$C(u) = \min_{q \in V} \{ \max\{C(q), d(q, u)\} \} \quad (10)$$

Where  $\forall q \in P$ ,  $C(q) = 0$  (prototypes have zero cost), and  $\forall q \in V$ ,  $C(q) = +\infty$ . (all other samples are initially assigned infinite cost). These costs are

used in the first iteration to initialize the algorithm. Below, the implementation steps of the OPF classifier are illustrated.

---

#### OPF classification algorithm [32]

---

**Input:** A learning set  $V$ , prototype set  $S(P) \subseteq V$ , distance function  $d$  and learning set label map  $\lambda$ .

**Output :**  $P$  Predecessors Map,  $C$  path cost map and  $L$  label map.

**Auxiliary:**  $Q$  Priority Queue,  $cst$  variable.

```

1  For all  $q \in V$  do
2       $P(q) \leftarrow \text{nil}, C(q) \leftarrow +\infty$ ;
3  End ;
4  For all  $q \in S$  do
5       $C(q) \leftarrow 0, L(q) = \lambda(q), Q \leftarrow q$ ;
6  End ;
7  While  $Q \neq \text{nil}$  do
8      Remove from  $Q$  a sample  $q$  such that  $C(q)$  is
        minimum;
9      For each sample  $u \in V$  such that  $q \neq u$  and
         $C(u) > C(q)$  do
10          $cst \leftarrow \max\{C(q), d(q, u)\}$ ;
11         If  $cst < C(u)$  then
12             If  $C(u) \neq +\infty$  then
13                 Remove  $u$  from  $Q$ ;
14             End ;
15              $L(u) \leftarrow L(q), P(u) \leftarrow q, C(u) \leftarrow cst$ ;
16              $Q \leftarrow u$ ;
17         End ;
18     End ;
19 End ;
20 Return  $[P, C, L]$  ;

```

---

According to the algorithm flow, the OPF training step initializes by assigning a cost of 0 to prototypes and  $+\infty$  to the remaining samples. Each sample has its predecessor set to nil, and prototypes are added to the priority queue  $Q$ . Starting from line 4, the algorithm iterates through all samples  $q \in V$  to conquer the remaining nodes. The core of the OPF algorithm lies in the main loop (lines 7–19), where a sample  $q$  with the minimum cost is removed from  $Q$ , and its neighborhood is analyzed. If the offered cost is greater than the current cost of a neighboring node  $u$ ,  $u$  is labeled with the same class as  $q$  and added to its tree [33].

To accelerate the OPF training phase, the competition process, governed by the supervised OPF using  $f_{max}$ , follows the structure of the Minimum Spanning Tree (MST). The final optimal path forest generated after training resembles computing the MST and then removing edges between prototypes, followed by propagating the costs of each prototype. Key points include:

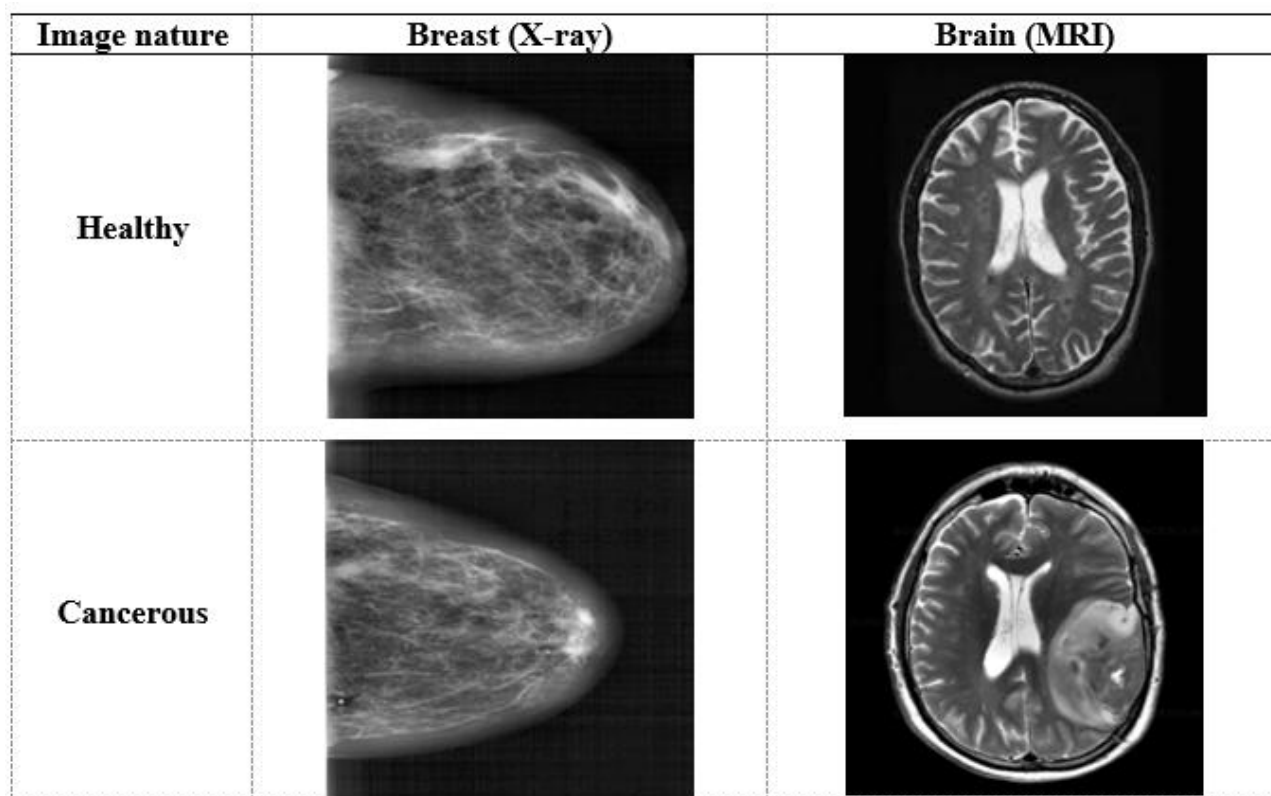


Figure. 4 Samples from the two medical image datasets

- There is only one possible MST when all arc weights are unique.

- No alternative path exists for a prototype to conquer a sample outside its class.

A similar procedure is applied to the evaluation set to ensure reliable class distribution in the feature space and enhance classification performance.

## 5. Experimental results and discussion

To demonstrate the effectiveness, reliability, and robustness of our proposed model for tumor detection and classification in medical images, extensive experiments are conducted using five datasets: three for mammographic images (DDSM, INbreast, and MIAS) and twice for brain images (Kaggle, Figshare). Each category includes a large number of samples from multiple datasets, ensuring the model is well-adapted to handle diverse variations in medical images. Fig. 4 illustrates sample images from these datasets used for model development and evaluation.

By utilizing these datasets, we aim to validate the generalizability and robustness of our proposed approach across various types of medical images, ensuring its applicability in real-world clinical scenarios.

- Breast datasets: consist of 24,576 X-ray images categorized into two classes: healthy and cancerous.

- Brain datasets: contain 3,064 and 3,264 brain MRI slices from Figshare and Kaggle, respectively, featuring three types of brain tumors: glioma, meningioma, and pituitary.

Fig. 4 visually represents example images from the two primary datasets used in this study: breast images and brain images. Each dataset is categorized based on the type of tumor or condition being analyzed, offering a clear illustration of the data used for training and evaluation. The figure highlights the diversity and complexity of the medical images, emphasizing the challenges in tumor detection and classification. It underscores the importance of robust preprocessing, feature extraction, and classification techniques in achieving accurate and reliable results in medical image analysis.

Tables 1 and 2 provide detailed descriptions of the breast and brain datasets, respectively, outlining their key characteristics and distributions. This diverse and extensive dataset collection ensures a rigorous evaluation of the proposed model, validating its effectiveness and robustness across various medical image types and tumor categories.

Before applying the proposed methods to the database images, a critical preprocessing step is performed to enhance image quality, which is essential for improving the model's precision and efficiency. The preprocessing phase includes three key steps:



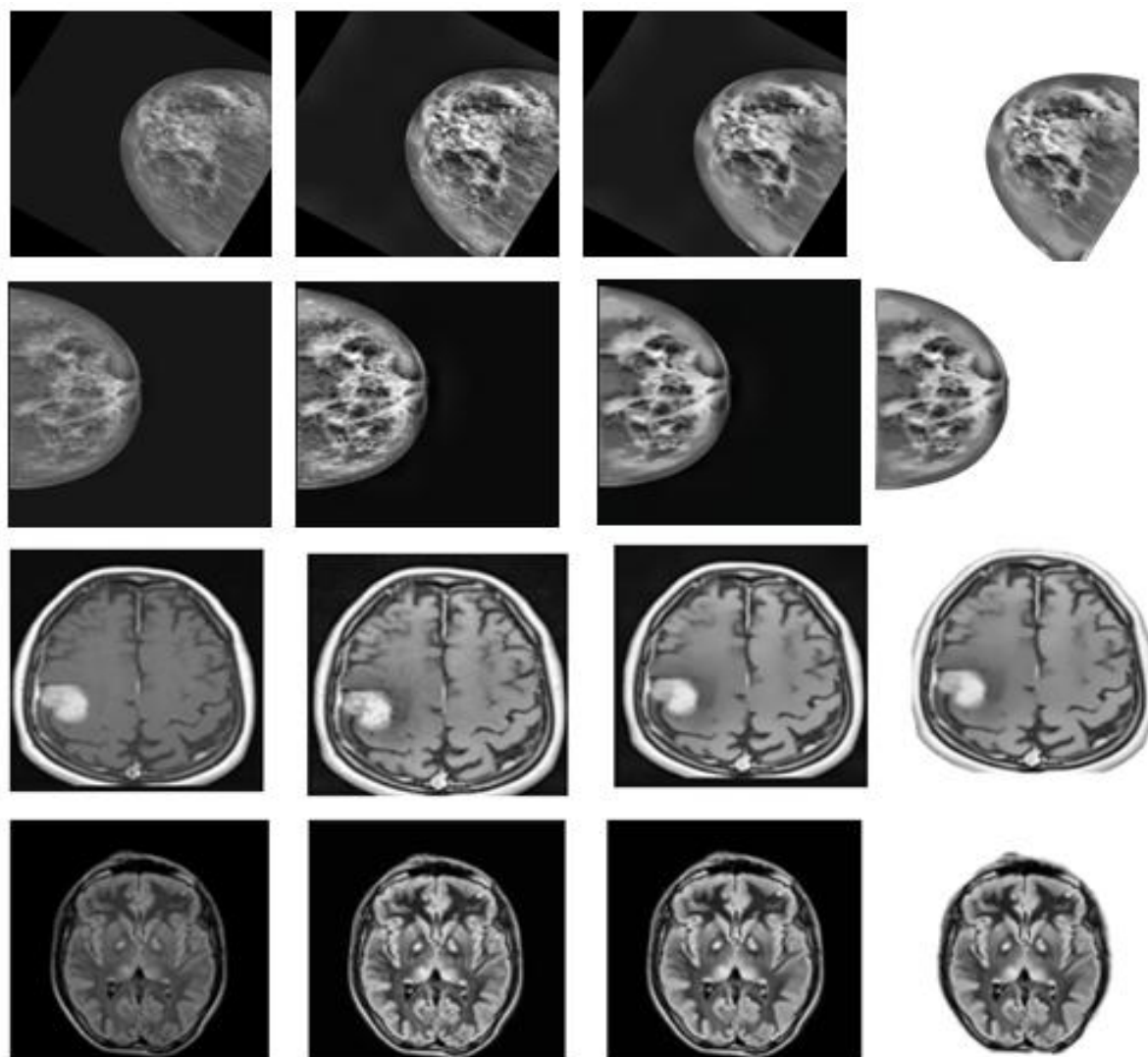


Figure. 5 The preprocessing process effect on the original brain and breast images: (First column) original images; (second column) equalization results images; (third column) noise-reduction results images; (fourth column) background-elimination results images

Table 1. Breast datasets detail

Breast datasets	Benign disease	Malignant disease
DDSM Dataset	5,970	7,158
INbreast Dataset	2,520	5,112
MIAS Dataset	2,376	1,440
Total images	10,866	13,710

Table 2. Brain datasets detail

Brain tumor type	Kaggle Dataset	Figshare Dataset
Pituitary	901	930
Glioma	926	1,426
Meningioma	937	708
Healthy masses	500	/
Cancerous masses	/	/
Total images	3,264	3,064

- **Histogram Equalization:** Adjusts image contrast by redistributing intensity values across the histogram, ensuring a balanced representation of pixel intensities.
- **Color Quantization:** Reduces the image's color space to a limited set of colors, simplifying the image while preserving essential features and reducing computational complexity and noise.
- **Local Contrast Enhancement:** Enhances contrast in specific regions, making subtle details more visible and improving overall image clarity.

These steps collectively prepare the images for more accurate and efficient analysis.

The visual representations in Fig. 5 clearly

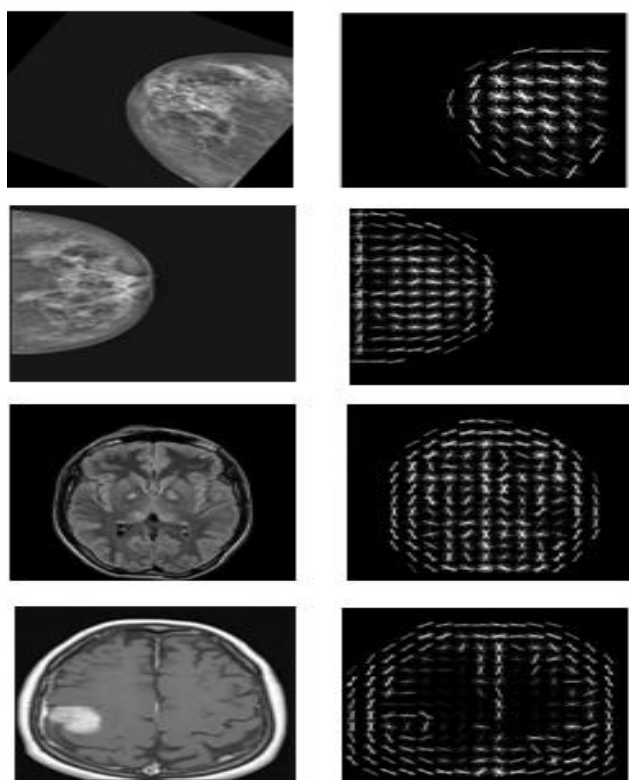


Figure. 6 Resulting images from the HOG feature extraction step

illustrate how each preprocessing step enhances the overall quality of the medical images, ensuring improved input for the subsequent feature extraction and classification processes.

The enhanced image from the final preprocessing step is used as input for the proposed model. Feature extraction is performed using the HOG, which computes local gradient orientations to capture texture and shape information. This process generates feature vectors that serve as input for the image classification model.

The goal is to create an accurate and efficient image classification system capable of distinguishing

between tumor types and non-tumor tissues. Extracted HOG features are used to train and test the classification model, improving tumor diagnosis and treatment. Fig. 6 demonstrates the results of the HOG feature extraction process, highlighting its effectiveness in capturing critical image features. By leveraging HOG, the proposed model ensures robust and reliable performance, making it highly applicable in real-world medical imaging scenarios.

For HOG to excel in feature extraction, the selection of parameters is carefully optimized to maximize performance. Several key parameters can be tuned to enhance the feature extraction process for specific applications:

- **Block Size:** The size of the blocks used to compute gradient histograms.
- **Number of Orientation Bins:** The number of bins used in the histogram to capture gradient orientations.
- **Cell Size:** The size of the cells used to compute gradient orientations within each block.
- **Block Overlap:** The degree of overlap between adjacent blocks.
- **Normalization Method:** The technique used to normalize the histogram values within each block.

By optimizing these parameters, the proposed model ensures that the extracted features are both discriminative and computationally efficient, enhancing the overall performance of the tumor detection and classification system.

Fig. 7 shows the resulting images for varying cell sizes, demonstrating the impact of this parameter on feature extraction. Table 3 provides a detailed analysis of how cell size affects the number of HOG features extracted from breast and brain images, highlighting the trade-offs between feature dimensionality and computational efficiency.

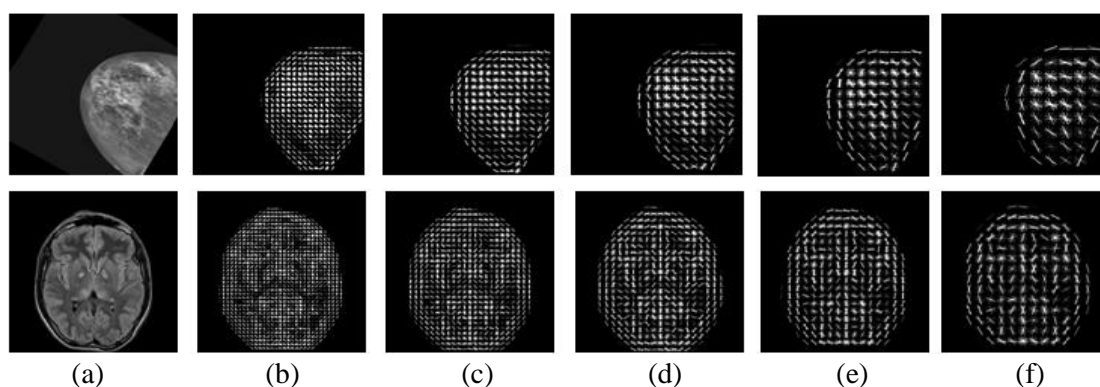


Figure. 7 Resulting images as a function of cell size: (a) input images, (b) image with HOG 6X6 cell size, (c) image with HOG 8X8 cell size, (d) image with HOG 10X10 cell size, (e) image with HOG 12X12 cell size, and (f) image with HOG 16X16 cell size

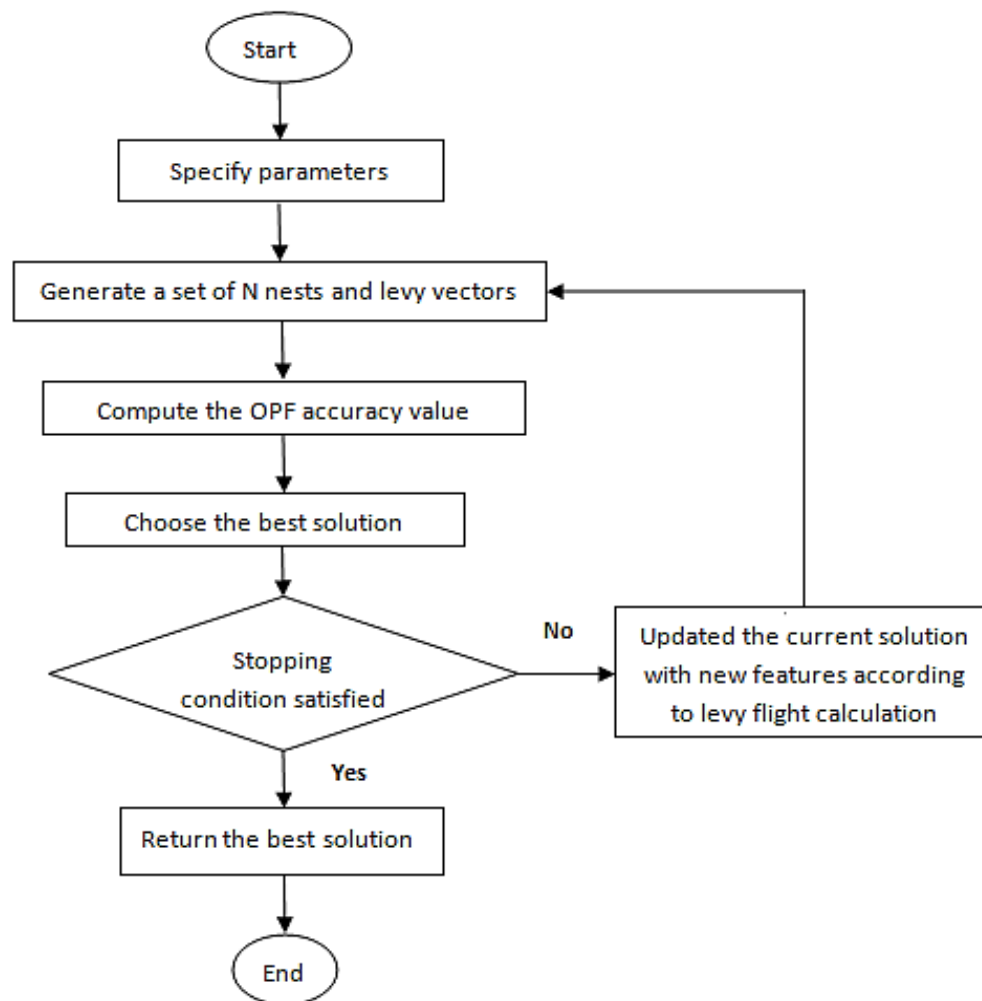


Figure. 8 Flowchart of the proposed methodology for the selection of the most relevant features via BCS algorithm

Table 3. HOG cell size effect on the features number provided from breast and brain images

Resulting images	Features number
(B)	29,520
(C)	16,740
(D)	9,504
(E)	6,480
(F)	3,780

Table 3 provides a detailed analysis of how varying the Histogram of Oriented Gradients (HOG) cell size impacts the number of features extracted from both breast and brain medical images.

The results presented above demonstrate that varying the HOG cell size significantly influences both the number of features extracted and the quality of the resulting image. Specifically, the HOG 16×16 cell size yields the best balance between image quality and the number of features, delivering the utmost performance. This configuration ensures a reduced feature dimensionality while maintaining

high-quality feature extraction, making it the most efficient choice for our proposed model.

By selecting the 16×16 cell size, the model achieves a compact yet highly discriminative feature set, enhancing computational efficiency without compromising accuracy. This choice underscores the importance of parameter optimization in maximizing the performance of the HOG descriptor for tumor detection and classification in medical images.

To strike a balance between avoiding an excessively large number of features and retaining critical information, the following recommended settings are applied:

- 9 orientation bins.
- Cell size of 16×16 pixels.
- Block size of 2×2 cells.

These settings result in 3,780 features for both brain and breast images, ensuring a compact yet comprehensive feature set that captures essential texture and shape information while maintaining computational efficiency. However, HOG feature extraction can produce an excessively large number

of features—each image yields 3,780 features, and with over 1,000 images per tumor type, computational complexity increases significantly. To address these challenges and enable efficient image detection and classification, optimization is essential.

Medical images contain highly relevant and sensitive information, making it essential to preserve critical features during optimization. The goal is to achieve accurate classification with improved efficiency and reduced processing time. To accomplish this, the Binary Cuckoo Search (BCS) algorithm is used for feature optimization, reducing dimensionality by selecting the most relevant and discriminative features while minimizing redundancy. By integrating BCS, the model balances feature reduction and classification accuracy, enabling robust and efficient tumor detection and classification. This optimization step enhances the model's practicality and performance in real-world applications.

The extracted HOG features are input into the BCS algorithm, which identifies and selects the most relevant and informative features. These selected features have the greatest impact on the accuracy of medical image classification. In BCS implementation, the OPF accuracy is used as the evaluation metric, serving as the objective function to guide the optimization process.

The best feature subset is determined by maximizing OPF accuracy rates for breast and brain datasets, ensuring optimal features for classification while balancing accuracy and computational efficiency. Fig. 8 details the proposed feature optimization method, illustrating how BCS refines the feature set to enhance classification performance.

By integrating BCS with OPF accuracy as the guiding metric, the model achieves a robust and efficient feature selection process, retaining the most significant features for accurate and reliable tumor detection and classification in medical images.

Through empirical analysis, the parameters for the BCS algorithm are carefully selected to achieve optimal performance. The configuration includes: 50 generations, each containing 10 solutions, resulting in a population size of 10 nests.

Tuning parameters:

- $\alpha = 1$  (scaling factor for step size),
- $\beta = 1.5$  (parameter for Lévy flight distribution),
- $\lambda = 2.5$  (parameter controlling the shape of the distribution).

This configuration ensures the algorithm efficiently explores the search space and converges to the best solution, balancing exploration and exploitation. By carefully tuning these parameters, the BCS algorithm achieves robust and efficient feature optimization, enhancing the accuracy and reliability of the proposed tumor detection and classification model.

The BCS algorithm achieves a significant reduction in the feature set, demonstrating its effectiveness in optimizing the feature space. Specifically:

- For the brain dataset, a subset of 1,085 features is selected per image, representing an optimization rate of 28.70%.
- For the breast dataset, a subset of 1,134 features is selected per image, representing an optimization rate of 30%.

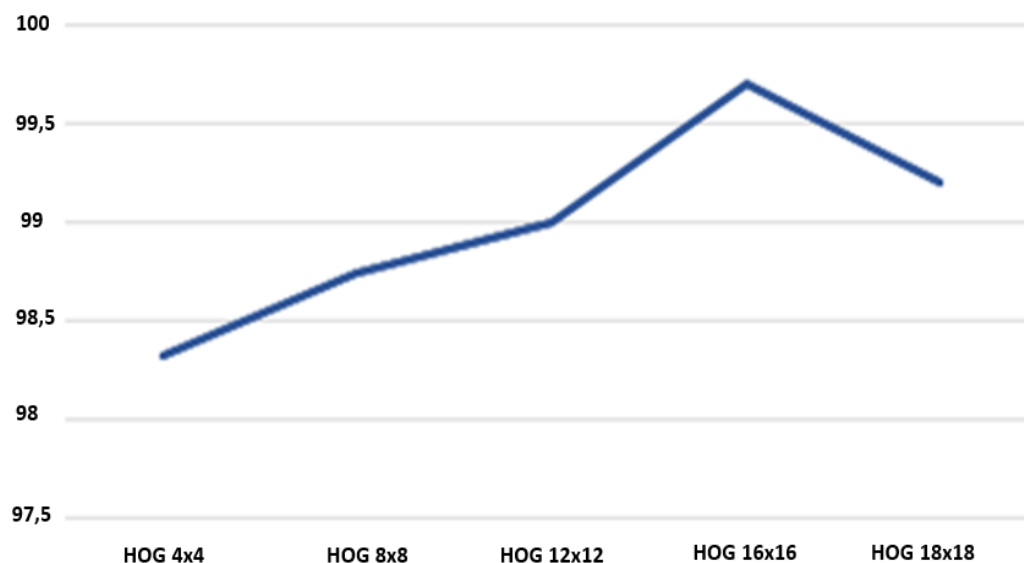


Figure. 9 Effect of HOG descriptor cell size on OPF accuracy

Table 4. A summary of BIA-FS invested in the medical field

Related work iteration	BIA	Improvement technique	Population	Max
Sathiyabhama et al. [34]	GWA	Rough set theory	22	None
Tahir et al. [35]	GA	Chaotic maps	30	50
Pasha and Latha [36]	GA, PSO	None	50	100
Nadimi-Shahraki et al. [37]	AQA	Levy flight	300	300
Elgamal et al. [38]	RSA	Chaotic maps	10	100
Preeti and Deep [39]	GWA	Random walk	10	100
Vijh et al. [40]	WHA	Hybridization	25	35
Zenbout et al. [41]	GWA	Initialization phase	11	300
<b>Proposed method</b>	<b>BCS</b>	<b>Lévy flight</b>	<b>10</b>	<b>50</b>

**Abbreviations:** AQA, aquila algorithm; BCS, binary cuckoo search; GA, genetic algorithms; GWA, grey wolf algorithm; PSO, particle swarm algorithm; RSA, reptile search algorithm; WHA, whale-inspired algorithm.

This optimized feature subset not only reduces the risk of overfitting but also enhances the classification accuracy of the model. It is important to note that the performance of the BCS optimization is highly dependent on the HOG cell size, which directly influences the OPF accuracy.

Fig. 9 illustrates the impact of varying HOG cell sizes on the OPF accuracy, highlighting the importance of selecting the optimal cell size for maximizing classification performance. By achieving a balance between feature reduction and accuracy, the proposed model ensures robust and efficient tumor detection and classification in medical images.

The analysis of the accuracy graph versus HOG cell size reveals that a HOG cell size of 16×16 delivers the highest accuracy for the Optimal-Path Forest (OPF) classifier when combined with the Binary Cuckoo Search (BCS). This suggests that a feature representation based on 16×16 HOG cells enables the OPF classifier to achieve superior performance in medical image classification tasks.

The optimal HOG cell size varies depending on the type of medical images (e.g., brain, breast) and the specific classification requirements. Factors like image resolution, texture complexity, and tumor characteristics influence the effectiveness of different cell sizes. Adapting the HOG cell size based on image characteristics and task context ensures robust and effective feature extraction across diverse medical imaging scenarios, enhancing the accuracy and reliability of the proposed model.

To demonstrate the performance and effectiveness of our proposed optimization method using the BCS, we provide a summary of various bio-inspired optimization methods for feature selection (BIA-FS) in the medical domain, as proposed in the literature. The table below compares these methods.

From the analysis of the BIA-FS methods cited in the above table, we can suggest that our proposed

optimization method via BCS performs better with a smaller population and a reduced number of iterations. This implies that our proposed model for medical image detection and classification exploiting BCS is rather insightful and quite effective.

Once the optimal feature subset is identified through the BCS optimization process, these features are input into the OPF algorithm to classify tumor types. By reducing input data dimensionality, the selected features enhance the robustness and computational efficiency of the OPF classifier, resulting in a more efficient and accurate image classification model.

The OPF algorithm is trained using the optimal feature subset, mapping each feature to its corresponding tumor type based on input images and ground truth annotations. This training process enables the algorithm to distinguish between metastatic cancer regions and non-infected regions, ensuring accurate tumor identification and classification. The optimized feature set improves both accuracy and efficiency in the classification process.

As shown in Figs. 10 and 11, the OPF algorithm effectively detects and classifies tumors in breast and brain images with high accuracy. These visualizations highlight the strength of the OPF algorithm in medical image analysis, particularly when combined with the optimized feature subset obtained through the BCS.

To evaluate the performance [34] and suitability of our proposed HOG-BCS-OPF model for tumor detection and classification in medical images, a comprehensive comparison has been conducted with various recent approaches from the literature. The comparison is based on accuracy, calculated using Formula 11.

$$\text{Accuracy} = \frac{TP+TN}{TP+FN+FP+TN} \quad (11)$$

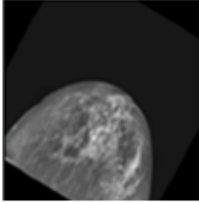
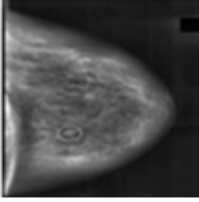
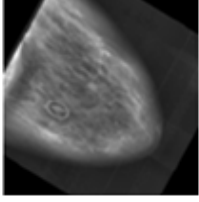
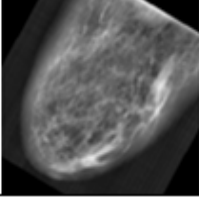
Sample dataset	Tumour nature	OPF prediction
	Benign	Benign
	Malignant	Malignant
	Malignant	Malignant
	Benign	Benign

Figure. 10 Tumor detection result in breast images by OPF

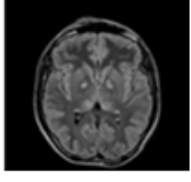
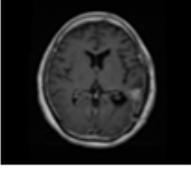
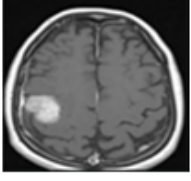
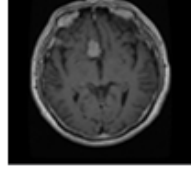
Sample dataset	Tumour nature	OPF prediction
	No tumour	No tumour
	Glioma tumour	Glioma tumour
	Meningioma tumour	Meningioma tumour
	Pituitary tumour	Pituitary tumour

Figure. 11 Tumor detection result in brain images by OPF



Where TP indicates true positive, TN represents true negative, FP denotes false positive, and FN describes false negative.

Table 5 and Table 6 provide a detailed comparison of our proposed model with other state-of-the-art models on breast and brain images, respectively, showcasing the superior accuracy and efficiency of the HOG-BCS-OPF model.

Additionally, the confusion matrix is used to illustrate the classification results of the model, which was pre-trained via OPF on the test set of breast and brain datasets, are shown in Figs. 12 and 13, respectively.

Figs. 12A, B and C present the evaluation metrics for breast tumor classification of the HOG-BCS-OPF model on DDSM, Inbreast and MIAS dataset, respectively. On the DDSM dataset, Fig. 12A shows that the combination of HOG, BCS, and OPF achieves the best classification accuracy, with a value of 99.73%. In Fig. 12B (i.e., INbreast dataset), the

HOG-BCS-OPF model also achieves the best performance with an accuracy of 97.31%. Fig. 12C illustrates the classification results of the model on MIAS dataset, which demonstrate an excellent accuracy of 93.85%. The experimental results validate the effectiveness of the HOG and BCS combination for feature extraction and selection, thus providing a more reliable approach for breast tumor classification using the OPF classifier.

Figs. 13A and B present the confusion matrices of the brain tumor classification results obtained by the HOG-BCS-OPF model on the Figshare and Kaggle dataset, respectively. Based on the Figshare dataset, Fig. 13A shows that the model achieves the best classification accuracy with a value of 97.72%, while Fig. 13B illustrates the classification results of the model on the Kaggle dataset, which displays an excellent accuracy of 93.57%. Hence, the success and effectiveness of our model for tumor detection and classification on brain MRI images.

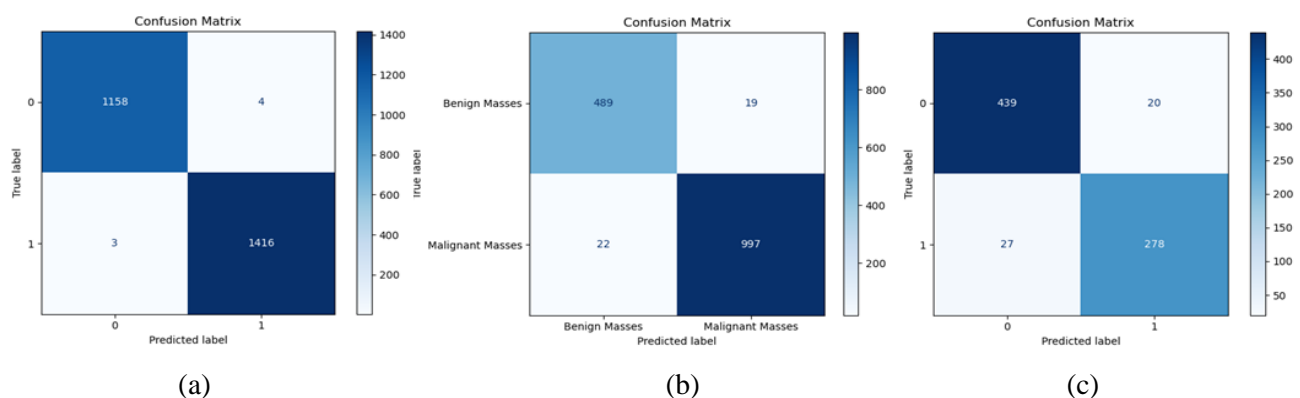


Figure. 12 Confusion matrix detail of the model on the test set of breast datasets: (a) DDSM dataset, (b) INbreast dataset, and (c) MIAS dataset

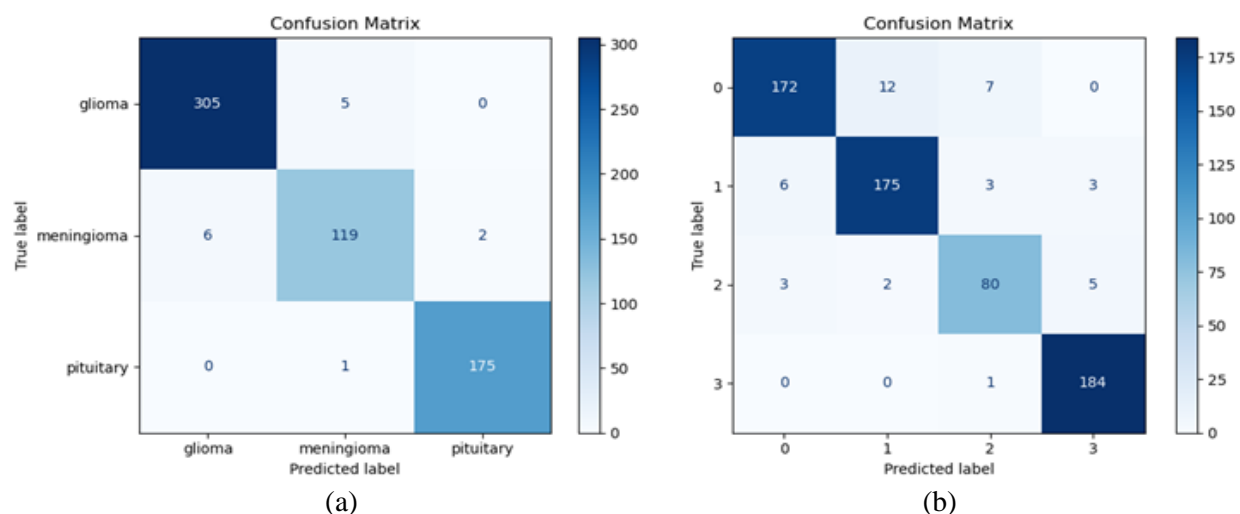


Figure. 13 Confusion matrix detail of the model on the test set of brain datasets: (a) Figshare dataset and (b) Kaggle dataset

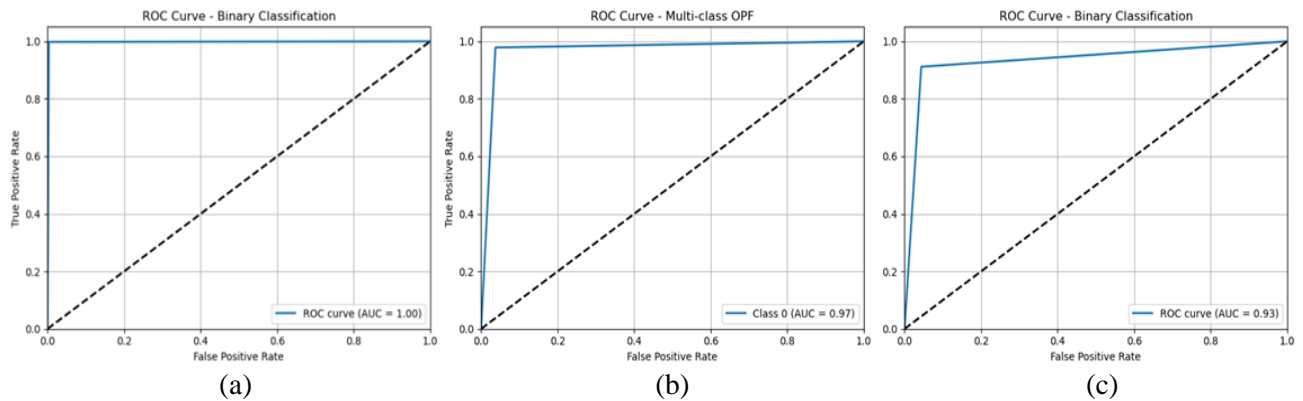


Figure. 14 AUC performance analysis of the model on breast datasets: (a) DDSM dataset, (b) INbreast dataset, and (c) MIAS dataset

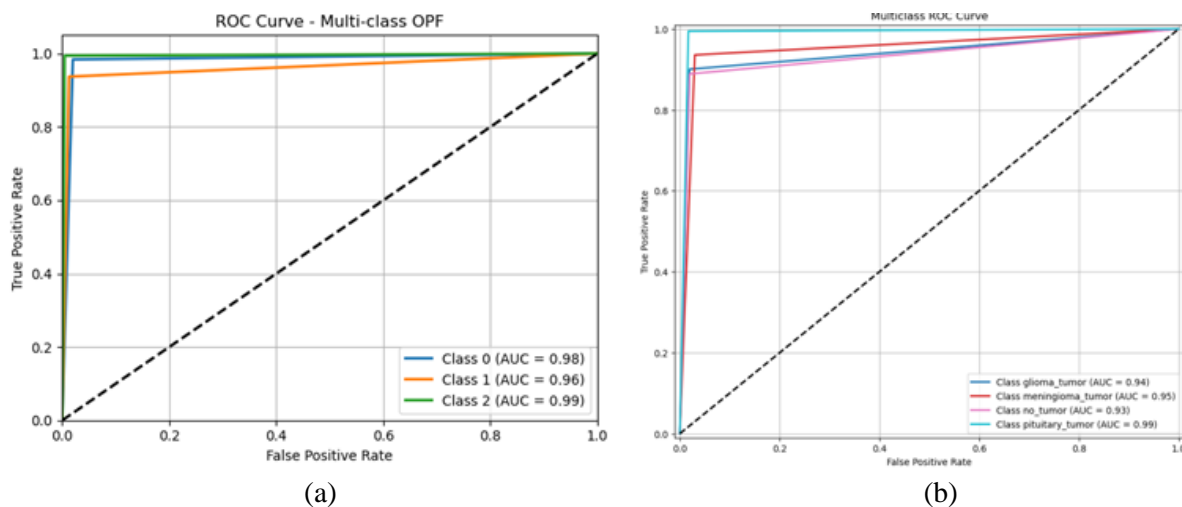


Figure. 15 AUC performance analysis of the model on brain datasets: (a) Figshare dataset and (b) Kaggle dataset

Table 5. Comparison of the proposed model with recent advanced techniques in breast imaging

Related work	Year	Datasets	Accuracy (%)
Ting et al. [42]	2019	MIAS	90.59
Falconi et al. [43]	2020	INbreast	90.90
Salama et al. [44]	2020	DDSM	97.98
El Houby and Yassin. [45]	2021	INbreast	96.52
		MIAS	93.39
Salama and aly. [46]	2021	DDSM	98.87
		MIAS	93.88
Merzoug et al. [47]	2022	MIAS	90.00
Muduli et al. [48]	2022	INbreast	91.28
Rahman et al. [49]	2023	INbreast	93.00
Yan et al. [50]	2023	DDSM	96.66
Abimouloud et al. [51]	2024	DDSM	99.05
Kumar et al. [52]	2025	DDSM	99.48
<b>Proposed model</b>		<b>MIAS</b>	<b>93.85</b>
		<b>INbreast</b>	<b>97.31</b>
		<b>DDSM</b>	<b>99.73</b>

A Receiver Operating Curve (ROC) is also used in the analysis process. This curve is useful for describing the results by illustrating the relationship between the true positive rate and the false positive rate. The size of the area under the curve (AUC) of the ROC curve signifies the model's ability to

categorize different tumor types; a higher AUC value indicates better classification performance. Figs. 14 and 15 illustrate the ROC curves of the HOG-BCS-OPF model on breast and brain images, respectively. Figs. 14A, B, and C illustrate the ROC curve of the model on the three datasets used for breast images.



Table 6. Comparison of the proposed model with recent advanced techniques in breast imaging

Related work	Year	Technique	Dataset	Accuracy (%)
Abiwinanda et al. [53]	2019	CNN	Figshare	84.19
Kabir Anaraki et al. [54]	2019	GA-CNN	Figshare	94.20
Kaplan et al. [55]	2020	LBP SVM KNN	Figshare	95.56
Kang et al. [56]	2021	Feature connection	Kaggle	91.80
Shahajad et al. [57]	2021	SVM	Kaggle	92.00
Vankdothu et al. [58]	2022	CNN-LSTM	Kaggle	92.00
Tummala et al. [59]	2022	Ensemble of ViTs	Figshare	97.71
Ahmad et al. [60]	2022	GAN-VAEs	Figshare	96.25
Hammad et al. [61]	2023	8-layer CNN	Figshare	96.86
Khaliki et Başarslan. [62]	2024	3-layer CNN	Kaggle	91.00
Gasmi et al. [63]	2024	ViTs+EfficientsNetV2	Figshare	96.09
<b>Proposed Model</b>		<b>HOG-BCS-OPF</b>	<b>Kaggle</b>	<b>93.57</b>
			<b>Figshare</b>	<b>97.72</b>

**Abbreviations:** EfficientNetB2, pre-trained network; GA, genetic algorithms; GAN-VAEs, Combination of Generative Adversarial Networks and Variational Autoencoders; KNN, K nearest neighbors; LBP, local binary patterns; LSTM, Long Short-Term Memory; PT-CNN, Pre-Trained Convolutional Neural Network; SVM, support vector machine; ViTs, Vision Transformers.

The AUC values for the DDSM (Fig. 14A), INbreast (Fig. 14B), and MIAS (Fig. 14C) datasets are 1, 0.97, and 0.93, respectively. Figs. 15A, B illustrate the ROC curve of the model on the two datasets used for brain images.

The AUC values for the three brain tumor types in the Figshare dataset (Fig. 15A) are 0.98, 0.96, and 0.99, respectively, and in the Kaggle dataset (Fig. 15B) are 0.94, 0.95 and 0.99, respectively.

According to Table 5, on the DDSM dataset, the HOG-BCS-OPF model achieves near-perfect classification performance for breast tumors with an accuracy of 99.73%, while on the INbreast and MIAS datasets, HOG-BCS-OPF shows excellent classification performance with an accuracy of 97.31% and 93.85%, respectively. In Table 6, the HOG-BCS-OPF model shows the best classification performance for brain tumors with an accuracy of 97.72% on the Figshare dataset, while on the Kaggle dataset, HOG-BCS-OPF shows excellent classification performance with an accuracy of 93.57%, outperforming many existing methods. The execution times (9.604 seconds for breast images and 13.740 seconds for brain images) demonstrate the model's computational efficiency, making it suitable for real-world clinical applications.

The comparison highlights the superiority of our model in terms of accuracy, speed and efficiency, underscoring its potential as a reliable tool for tumor detection and classification in medical imaging.

These results validate the effectiveness of the HOG-BCS-OPF model and its applicability across different types of medical images, ensuring high diagnostic accuracy and practical utility in healthcare settings.

## 6. Conclusion and future work

The primary objective of this study was to develop a robust model for classifying medical images based on tumor types. This involved two distinct classification tasks: binary classification for mammographic images to differentiate between benign and malignant tumors, and multi-class classification for brain images to categorize tumors into three types: glioma, meningioma, and pituitary tumor. To achieve this, the proposed model follows a two-stage processing pipeline.

In the first stage, efficient preprocessing is applied to raw medical images to enhance their quality, resulting in more interpretable and computationally efficient images. Subsequently, the Histogram of Oriented Gradients (HOG) technique is

employed to extract comprehensive and precise features from the enhanced images. However, the large number of features generated by HOG necessitates optimization to refine the classification process. To address this, the Binary Cuckoo Search (BCS) algorithm is utilized, ensuring an optimal and relevant feature set while maintaining low computational cost and fast convergence speed.

In the second stage, the optimized feature subset is fed into the Optimal-Path Forest (OPF) classifier, a highly efficient technique for image classification. The OPF classifier delivers excellent, reliable, and robust classification results, effectively highlighting tumor regions in both breast and brain cells.

The proposed model was evaluated on two distinct datasets: one dedicated to breast images and the other to brain images. The model achieved remarkable accuracy rates of 99.73% for breast image classification and 97.72% for brain image classification, outperforming several state-of-the-art methods in medical image analysis. These results underscore the robustness, reliability, and relevance of the proposed HOG-BCS-OPF model.

For future research, the model can be further enhanced by hybridizing BCS with other popular bio-inspired algorithms (BIAs), such as the Particle Swarm Optimization (PSO) and Grey Wolf Optimizer (GWO). Such hybridization could potentially improve feature selection and classification performance, opening new avenues for advancements in medical image analysis.

### Data availability statement

Publicly available datasets were analyzed in this study. This data can be accessed at:

DDSM: <https://www.kaggle.com/skooch/ddsm-mammography>;

INbreast: <https://www.kaggle.com/datasets/tommyngx/inbreast2012>;

MIAS: <https://www.kaggle.com/datasets/kmader/mias-mammography>;

Figshare: [https://figshare.com/articles/dataset/brain\\_tumor\\_dataset/1512427](https://figshare.com/articles/dataset/brain_tumor_dataset/1512427);

and Kaggle: <https://www.kaggle.com/datasets/sartajbhuvaji/brain-tumor-classification-mri>.

### Abbreviations definition

ANN Artificial Neural Network  
BCS Binary Cuckoo Search  
BIAs Bio-Inspired Algorithms

CAD Computer-Aided Diagnosis  
CNNs Convolutional Neural Networks  
CS Cuckoo Search  
DT Decision Tree  
FA Firefly Algorithm  
GCN Graph Convolutional Network  
GWO Grey Wolf Optimizer  
HOG Histogram of Oriented Gradients  
KNN K-nearest neighbor  
MRI Magnetic Resonance Image  
OPF Optimum Path Forest  
PSO Particle Swarm Optimization  
RGA region growing algorithm  
SVM Support Vector Machine  
ViTs Vision Transformers

### Conflicts of Interest

The authors declare no conflict of interest.

### Author Contributions

Conceptualization, N. Chaoui, and B. Meftah; methodology, N. Chaoui, B. Meftah, and A. Ghomari; software, N. Chaoui; validation, N. Chaoui, B. Meftah, and A. Ghomari; formal analysis, B. Meftah; writing—original draft preparation, N. Chaoui, and B. Meftah; writing—review and editing, B. Meftah, and A. Ghomari; supervision, B. Meftah, and A. Ghomari.

### References

- [1] N. Azamjah, Y. Soltan-Zadeh, and F. Zayeri, "Global Trend of Breast Cancer Mortality Rate: A 25-Year Study", *Asian Pacific Journal of Cancer Prevention*, Vol. 20, No. 7, pp. 2015-2020, 2019.
- [2] V. B. Babu, S. Srinivasan, S. K. Mathivanan, Mahalakshmi, P. Jayagopal, and G. T. Dalu, "Detection and Classification of Brain Tumor Using Hybrid Deep Learning Models", *Scientific Reports*, Vol. 13, No. 1, p. 23029, 2023.
- [3] G. G. Boumediene, S. Benyahia, and B. Meftah, "An Optimized Clustering Approach Using Tree Seed Algorithm for the Brain MRI Images Segmentation", *Inteligencia Artificial*, pp. 44-59, 2023.
- [4] M. Arif, F. Ajesh, S. Shamsudheen, O. Geman, D. Izdrui, and D. Vicoveanu, "Brain Tumor Detection and Classification by MRI Using Biologically Inspired Orthogonal Wavelet Transform and Deep Learning Techniques", *Journal of Healthcare Engineering*, Vol. 2022, p. 2693621, 2022.

- [5] S. Natarajan, P. Sampath, R. Arunachalam, V. Shanmuganathan, G. Dhiman, P. Chakrabarti, et al., "Early Diagnosis and Meta-Agnostic Model Visualization of Tuberculosis Based on Radiography Images", *Scientific Reports*, Vol. 13, 2023.
- [6] P. B. Chanda and S. K. Sarkar, "Detection and Classification of Breast Cancer in Mammographic Images Using Efficient Image Segmentation Technique", *Lecture Notes in Electrical Engineering*, Vol. 591, pp. 107-117, 2020.
- [7] A. R. Venmathi, E. N. Ganesh, and N. Kumaratharan, "A Review of Medical Image Classification and Evaluation Methodology for Breast Cancer Diagnosis with Computer Aided Mammography", *International Journal of Applied Engineering Research*, Vol. 10, No. 1, pp. 30045-30054, 2015.
- [8] K. Jabeen, M. A. Khan, J. Balili, M. Alhaisoni, N. A. Almujaally, H. Alrashidi, et al., "BC2NetRF: Breast Cancer Classification from Mammogram Images Using Enhanced Deep Learning Features and Equilibrium-Jaya Controlled Regula Falsi-Based Features Selection", *Diagnostics*, Vol. 13, No. 7, p. 1238, 2023.
- [9] D. Wu, J. Ni, W. Fan, Q. Jiang, L. Wang, L. Sun, et al., "Opportunities and Challenges of Computer Aided Diagnosis in New Millennium: A Bibliometric Analysis from 2000 to 2023", *Medicine*, Vol. 102, No. 51, p. e36703, 2023.
- [10] K. Loizidou, R. Elia, and C. Pitris, "Computer-Aided Breast Cancer Detection and Classification in Mammography: A Comprehensive Review", *Computers in Biology and Medicine*, Vol. 153, p. 106554, 2023.
- [11] K. Erdem, M. A. Kobat, M. N. Bilen, Y. Balik, S. Alkan, F. Cavlak, et al., "Hybrid-Patch-Alex: A New Patch Division and Deep Feature Extraction-Based Image Classification Model to Detect COVID-19, Heart Failure, and Other Lung Conditions Using Medical Images", *International Journal of Imaging Systems and Technology*, Vol. 33, No. 4, p. 114459, 2023.
- [12] C. N. Chaoui, A. Ghomari, and B. Meftah, "Edge and Anomaly Detection of Brain Magnetic Resonance Images in a Distributed Environment", *International Journal of Imaging Systems and Technology*, Vol. 32, No. 2, pp. 642-657, 2022.
- [13] D. Wang, A. Khosla, R. Gargeya, H. Irshad, and A. Beck, "Deep Learning for Identifying Metastatic Breast Cancer", *arXiv:1606.05718*, 2016.
- [14] B. Ehteshami Bejnordi, M. Veta, P. J. van Diest, B. van Ginneken, N. Karssemeijer, G. Litjens, et al., "Diagnostic Assessment of Deep Learning Algorithms for Detection of Lymph Node Metastases in Women with Breast Cancer", *Journal of the American Medical Association*, Vol. 318, No. 22, pp. 2199-2210, 2017.
- [15] A. Carriero, L. Groenhoff, E. Vologina, P. Basile, and M. Albera, "Deep Learning in Breast Cancer Imaging: State of the Art and Recent Advancements in Early 2024", *Diagnostics*, Vol. 14, No. 8, p. 848, 2024.
- [16] T. Mathew, B. Ajith, J. R. Kini, and J. Rajan, "Deep Learning-Based Automated Mitosis Detection in Histopathology Images for Breast Cancer Grading", *International Journal of Imaging Systems and Technology*, Vol. 32, No. 4, pp. 1192-1208, 2022.
- [17] H. Zain Eldin, S. A. Gamel, E. S. M. El-Kenawy, A. H. Alharbi, D. S. Khafaga, A. Ibrahim, et al., "Brain Tumor Detection and Classification Using Deep Learning and Sine-Cosine Fitness Grey Wolf Optimization", *Bioengineering*, Vol. 10, No. 1, p. 18, 2023.
- [18] M. Agarwal, G. Rani, A. Kumar, P. K. K. R. Manikandan, and A. H. Gandomi, "Deep Learning for Enhanced Brain Tumor Detection and Classification", *Results in Engineering*, Vol. 22, p. 102117, 2024.
- [19] V. K. Dhakshnamurthy, M. Govindan, K. Sreerangan, M. D. Nagarajan, and A. Thomas, "Brain Tumor Detection and Classification Using Transfer Learning Models", *Engineering Proceedings*, Vol. 62, No. 1, p. 1, 2024.
- [20] W. Zhou, S. Gao, L. Zhang, and X. Lou, "Histogram of Oriented Gradients Feature Extraction from Raw Bayer Pattern Images", *IEEE Transactions on Circuits and Systems II: Express Briefs*, Vol. 67, No. 5, pp. 946-950, 2020.
- [21] X. S. Yang, *Nature-Inspired Metaheuristic Algorithms*, 2nd ed. Luniver Press, 2010.
- [22] M. R. Feizi-Derakhsh and E. A. Kadhim, "An Improved Binary Cuckoo Search Algorithm for Feature Selection Using Filter Method and Chaotic Map", *Journal of Applied Science and Engineering*, Vol. 26, No. 6, pp. 895-901, 2022.
- [23] L. Pereira, D. Rodrigues, T. Almeida, C. Ramos, A. Souza, X. S. Yang, et al., "A Binary Cuckoo Search and Its Application for Feature Selection", *Studies in Computational Intelligence*, pp. 141-154, 2014.
- [24] A. S. Iwashita, J. P. Papa, A. N. Souza, A. X. Falcão, R. A. Lotufo, V. M. Oliveira, et al., "A Path- and Label-Cost Propagation Approach to

- Speedup the Training of the Optimum-Path Forest Classifier”, *Pattern Recognition Letters*, Vol. 40, pp. 121-127, 2014.
- [25] J. P. Papa, A. X. Falcão, V. H. C. de Albuquerque, and J. M. R. S. Tavares, “Efficient Supervised Optimum-Path Forest Classification for Large Datasets”, *Pattern Recognition*, Vol. 45, No. 1, pp. 512-520, 2012.
- [26] R. W. R. de Souza, J. V. C. de Oliveira, L. A. Passos, W. Ding, J. P. Papa, and V. H. C. de Albuquerque, “A Novel Approach for Optimum-Path Forest Classification Using Fuzzy Logic”, *IEEE Transactions on Fuzzy Systems*, Vol. 28, No. 12, pp. 3076-3086, 2020.
- [27] N. Dalal and B. Triggs, “Histograms of Oriented Gradients for Human Detection”, In: *Proc. of IEEE Conference on Computer Vision and Pattern Recognition (CVPR’05)*, San Diego, CA, USA, pp. 886-893, 2005.
- [28] X. S. Yang and S. Deb, “Cuckoo Search via Lévy Flights”, In: *Proc. of World Congress on Nature & Biologically Inspired Computing (NaBIC)*, Coimbatore, India, pp. 210-214, 2009.
- [29] R. Abu Khurma, I. Aljarah, A. Sharieh, M. Abd Elaziz, R. Damaševičius, and T. Krilavičius, “A Review of the Modification Strategies of the Nature Inspired Algorithms for Feature Selection Problem”, *Mathematics*, Vol. 10, No. 3, p. 464, 2022.
- [30] J. P. Papa, A. X. Falcão, V. H. C. de Albuquerque, and J. M. R. S. Tavares, “Efficient Supervised Optimum-Path Forest Classification for Large Datasets”, *Pattern Recognition*, Vol. 45, No. 1, pp. 512-520, 2012.
- [31] J. P. Papa and A. X. Falcão, “A Learning Algorithm for the Optimum-Path Forest Classifier”, *Graph-Based Representations in Pattern Recognition*, Vol. 5534, pp. 195-204, 2009.
- [32] R. Souza, J. de Oliveira, L. Passos Júnior, W. Ding, J. Papa, and V. Albuquerque, “A Novel Approach for Optimum-Path Forest Classification Using Fuzzy Logic”, *IEEE Transactions on Fuzzy Systems*, Vol. 28, pp. 3076-3086, 2020.
- [33] J. P. Papa, S. E. N. Fernandes, and A. X. Falcão, “Optimum-Path Forest Based on k-Connectivity: Theory and Applications”, *Pattern Recognition Letters*, Vol. 87, pp. 117-126, 2017.
- [34] B. Sathiyabhama, S. U. Kumar, J. Jayanthi, T. Sathiya, A. K. Ilavarasi, V. Yuvarajan, et al., “A Novel Feature Selection Framework Based on Grey Wolf Optimizer for Mammogram Image Analysis”, *Neural Computing and Applications*, Vol. 33, No. 21, pp. 14583-14602, 2021.
- [35] M. Tahir, A. Tubaishat, F. Al-Obeidat, B. Shah, Z. Halim, and M. Waqas, “A Novel Binary Chaotic Genetic Algorithm for Feature Selection and Its Utility in Affective Computing and Healthcare”, *Neural Computing and Applications*, Vol. 34, No. 14, pp. 11453-11474, 2022.
- [36] A. Pasha and P. H. Latha, “Bio-Inspired Dimensionality Reduction for Parkinson’s Disease (PD) Classification”, *Health Information Science and Systems*, Vol. 8, No. 1, p. 13, 2020.
- [37] M. H. Nadimi-Shahraki, S. Taghian, S. Mirjalili, and L. Abualigah, “Binary Aquila Optimizer for Selecting Effective Features from Medical Data: A COVID-19 Case Study”, *Mathematics*, Vol. 10, No. 11, p. 1929, 2022.
- [38] Z. Elgamal, A. Q. M. Sabri, M. Tubaishat, D. Tubaishat, S. N. Makhadmeh, and O. A. Alomari, “Improved Reptile Search Optimization Algorithm Using Chaotic Map and Simulated Annealing for Feature Selection in Medical Field”, *IEEE Access*, Vol. 10, pp. 51428-51446, 2022.
- [39] Preeti and K. Deep, “A Random Walk Grey Wolf Optimizer Based on Dispersion Factor for Feature Selection on Chronic Disease Prediction”, *Expert Systems with Applications*, Vol. 206, p. 117864, 2022.
- [40] S. Vijh, P. Gaurav, and H. M. Pandey, “Hybrid Bio-Inspired Algorithm and Convolutional Neural Network for Automatic Lung Tumor Detection”, *Neural Computing and Applications*, Vol. 35, No. 33, pp. 23711-23724, 2023.
- [41] I. Zenbout, A. Bouramoul, S. Meshoul, and M. Amrane, “Efficient Bioinspired Feature Selection and Machine Learning Based Framework Using Omics Data and Biological Knowledge Data Bases in Cancer Clinical Endpoint Prediction”, *IEEE Access*, Vol. 11, pp. 2674-2699, 2023.
- [42] F. F. Ting, Y. J. Tan, and K. S. Sim, “Convolutional Neural Network Improvement for Breast Cancer Classification”, *Expert Systems with Applications*, Vol. 120, pp. 103-115, 2019.
- [43] L. Falconi, M. Perez, W. Aguilar, and A. Conci, “Transfer Learning and Fine Tuning in Mammogram BI-RADS Classification”, In: *Proc. of IEEE International Symposium on Computer-Based Medical Systems (CBMS)*, Rochester, MN, pp. 475-480, 2020.
- [44] W. M. Salama, A. M. Elbagoury, and M. H. Aly, “Novel Breast Cancer Classification Framework

- Based on Deep Learning”, *IET Image Processing*, Vol. 14, No. 13, pp. 3254-3259, 2020.
- [45] E. M. F. El Houbay and N. I. R. Yassin, “Malignant and Nonmalignant Classification of Breast Lesions in Mammograms Using Convolutional Neural Networks”, *Biomedical Signal Processing and Control*, Vol. 70, p. 102954, 2021.
- [46] W. M. Salama and M. H. Aly, “Deep Learning in Mammography Images Segmentation and Classification: Automated CNN Approach”, *Alexandria Engineering Journal*, Vol. 60, No. 5, pp. 4701-4709, 2021.
- [47] H. Merzoug, H. Yedjour, and S. Chouraqui, “A Deep System for Breast Tumor Classification from Mammograms”, *International Journal on Communications Antenna and Propagation*, Vol. 12, No. 6, pp. 394-403, 2022.
- [48] D. Muduli, R. Dash, and B. Majhi, “Automated Diagnosis of Breast Cancer Using Multi-Modal Datasets: A Deep Convolution Neural Network Based Approach”, *Biomedical Signal Processing and Control*, Vol. 71, p. 102825, 2022.
- [49] H. Rahman, T. F. Naik Bukht, R. Ahmad, A. Almadhor, and A. R. Javed, “Efficient Breast Cancer Diagnosis from Complex Mammographic Images Using Deep Convolutional Neural Network”, *Computational Intelligence and Neuroscience*, Vol. 2023, p. 7717712, 2023.
- [50] F. Yan, H. Huang, W. Pedrycz, and K. Hirota, “Automated Breast Cancer Detection in Mammography Using Ensemble Classifier and Feature Weighting Algorithms”, *Expert Systems with Applications*, Vol. 227, p. 120282, 2023.
- [51] M. L. Abimouloud, K. Bensid, M. Elleuch, O. Aiadi, and M. Kherallah, “Vision Transformer-Convolution for Breast Cancer Classification Using Mammography Images: A Comparative Study”, *International Journal of Hybrid Intelligent Systems*, Vol. 20, No. 2, pp. 67-83, 2024.
- [52] V. Kumar, K. C. T, N. P. Jagini, K. V. Rajkumar, R. K. Godi, and P. Tumuluru, “Enhanced Breast Cancer Detection and Classification via CAMR-Gabor Filters and LSTM: A Deep Learning-Based Method”, *Egyptian Informatics Journal*, Vol. 29, p. 100602, 2025.
- [53] N. Abiwinanda, M. Hanif, S. T. Hesaputra, A. Handayani, and T. R. Mengko, “Brain Tumor Classification Using Convolutional Neural Network”, In: *Proc. of World Congress on Medical Physics and Biomedical Engineering*, Vol. 68 No. 1, pp. 183-189, 2019.
- [54] A. K. Anaraki, M. Ayati, and F. Kazemi, “Magnetic Resonance Imaging-Based Brain Tumor Grades Classification and Grading via Convolutional Neural Networks and Genetic Algorithms”, *Biocybernetics and Biomedical Engineering*, Vol. 39, No. 1, pp. 63-74, 2019.
- [55] K. Kaplan, Y. Kaya, M. Kuncan, and H. M. Ertunç, “Brain Tumor Classification Using Modified Local Binary Patterns (LBP) Feature Extraction Methods”, *Medical Hypotheses*, Vol. 139, p. 109696, 2020.
- [56] J. Kang, Z. Ullah, and J. Gwak, “MRI-Based Brain Tumor Classification Using Ensemble of Deep Features and Machine Learning Classifiers”, *Sensors*, Vol. 21, No. 6, p. 2222, 2021.
- [57] M. Shahajad, D. Gambhir, and R. Gandhi, “Features Extraction for Classification of Brain Tumor MRI Images Using Support Vector Machine”, In: *Proc. of International Conference on Cloud Computing, Data Science & Engineering (Confluence)*, pp. 767-772, 2021.
- [58] R. Vankdothu, M. A. Hameed, and H. A. Fatima, “A Brain Tumor Identification and Classification Using Deep Learning Based on CNN-LSTM Method”, *Computers & Electrical Engineering*, Vol. 101, p. 107960, 2022.
- [59] S. Tummala, S. Kadry, S. A. C. Bukhari, and H. T. Rauf, “Classification of Brain Tumor from Magnetic Resonance Imaging Using Vision Transformers Ensembling”, *Current Oncology*, Vol. 29, No. 10, pp. 7498-7511, 2022.
- [60] B. Ahmad, J. Sun, Q. You, V. Palade, and Z. Mao, “Brain Tumor Classification Using a Combination of Variational Autoencoders and Generative Adversarial Networks”, *Biomedicines*, Vol. 10, No. 2, p. 223, 2022.
- [61] M. Hammad, M. ElAffendi, A. A. Ateya, and A. A. Abd El-Latif, “Efficient Brain Tumor Detection with Lightweight End-to-End Deep Learning Model”, *Cancers*, Vol. 15, No. 10, p. 2837, 2023.
- [62] M. Z. Khaliki and M. S. Başarslan, “Brain Tumor Detection from Images and Comparison with Transfer Learning Methods and 3-Layer CNN”, *Scientific Reports*, Vol. 14, No. 1, p. 2664, 2024.
- [63] K. Gasmi, N. Ben Aoun, K. Alsalem, I. B. Ltaifa, I. Alrashdi, L. B. Ammar, et al., “Enhanced Brain Tumor Diagnosis Using Combined Deep Learning Models and Weight Selection Technique”, *Frontiers in Neuroinformatics*, Vol. 18, p. 1444650, 2024.